

Universal quantum gates, artificial neurons and pattern recognition simulated by LC resonators

Motohiko Ezawa

Department of Applied Physics, University of Tokyo, Hongo 7-3-1, 113-8656, Japan

We propose to simulate quantum gates by LC resonators, where the amplitude and the phase of the voltage describe the quantum state. By controlling capacitance or inductance of resonators, it is possible to control the phase of the voltage arbitrarily. A set of resonators acts as the phase-shift, the Hadamard and the CNOT gates. They constitute a set of universal quantum gates. We also discuss an application to an artificial neuron. As an example, we study a pattern recognition of numbers and alphabets by evaluating the similarity between an input and the reference pattern. We also study a colored pattern recognition by using a complex neural network.

I. INTRODUCTION

Quantum computation is one of the most exciting fields of current physics¹⁻³. It is realized in various systems including superconductors⁴, photonic systems⁵, quantum dots⁶, trapped ions⁷ and nuclear magnetic resonance^{8,9}. For universal quantum computation, it is well known that only three quantum gates are enough, which are the phase-shift, the Hadamard and the CNOT gates¹⁰⁻¹².

Recently, electric circuits attract renewed attention in the context of topological physics¹³⁻²⁶. There are also some attempts to simulate various quantum gates by electric circuits²⁷⁻²⁹. Among them, a network of telegrapher lines is capable to simulate the universal quantum gates^{27,28}, because we may rewrite the Kirchhoff law in the form of the Schrödinger equation³⁰. This formulation requires long wires for a long quantum algorithm, where quantum states evolve spatially from the left wires to the right wires.

Quantum machine learning is an emerging field of contemporary physics³¹⁻⁴². Neural networks are often used in machine learning, where artificial neurons are basic elements^{43,44}. An artificial neuron has an internal degree of freedom called the weight. The output is determined from the input data by taking the inner product between the input data and the weight, and by applying an activation function to it. The inner product of two objects measures the similarity between them. For instance, using a series of numbers representing a reference pattern as the weight, we may analyze the similarity between an input pattern and the reference pattern as an output. Artificial neuron is simulated by quantum computer⁴⁵⁻⁵¹. Taking the inner product is the heaviest process, which will be executable by a quantum computer^{48,52}.

In this paper, we propose to simulate one qubit by a pair of LC resonators, where a set of voltage and current represents a wave function. First, we construct a phase-shift gate with an arbitrary phase by tuning the capacitance of an LC resonator. Next, we construct the Hadamard gate by tuning the inductance of an inductor bridging two LC resonators. We also construct the CNOT and the controlled phase-shift gate by using a voltage-controlled inductor or capacitor. Finally, we discuss applications to artificial neuron and pattern recognition. The calculation of the inner product may be executed by the operation of LC resonators for arbitrary inputs and weights. We elucidate the difference between the standard quantum-circuit implementation and the present electric-circuit implementa-

tion of the inner product.

This paper is composed as follows. In Sec.II, we start with a discussion how to store the information of N qubits $|j\rangle\rangle \equiv |n_1 n_2 \cdots n_N\rangle$ in a set of LC resonators, where $n_i = 0, 1$. Then, we propose to construct various quantum gates including a set of universal quantum gates by LC resonators.

In Sec.III, we apply our formalism to study artificial neurons, where we express various data with the aid of so-called real equally weighted (REW) states⁵³⁻⁵⁵. They are superposition states of N -qubits with coefficients $\alpha_j = \pm 1/\sqrt{2^N}$. In Sec.IV, we discuss a pattern recognition by calculating the inner product of an input data and the reference data. We present explicit examples of number recognition and alphabet recognition.

In Sec.V, we generalize REW states to include complex coefficients $\alpha_j = e^{i\theta_j}/\sqrt{2^N}$. We call them complex equally weighted (CEW) states. Then, we introduce complex-artificial neurons to deal with the inner product of CEW states. In Sec.VI, we propose to represent a colored pattern by a CEW state, where colored pattern recognition is done by evaluating the inner product of two CEW states representing the reference and an input pattern.

In Sec.VII, we present an electric-circuit implementation of quantum gates for calculation of an inner product starting from the initial N -qubit state $|00 \cdots 0\rangle$.

In Sec.VIII, we explore REW states from a viewpoint of graph and hypergraph states. We also introduce weighted graph and hypergraph states to represent CEW states. Sec.IX is devoted to discussions.

II. LC RESONATORS, QUBITS AND GATES

We use a set of 2^N identical LC resonators to simulate N -qubit quantum computation. An instance of $N = 2$ is illustrated in Fig.1(a). The voltage of the j th LC resonator is expressed as

$$V_j(t) = V_j^0 \cos(\omega_0 t + \theta_j), \quad (1)$$

where $\omega_0 = 1/\sqrt{LC}$ is the resonant frequency, V_j^0 is the absolute value of the voltage and θ_j is the phase shift.

A qubit state is defined by a superposition of the two states $|0\rangle$ and $|1\rangle$ as $|\psi\rangle = \alpha_0 |0\rangle + \alpha_1 |1\rangle$. Similarly, an N -qubit

state is defined by a superposition of the 2^N states as

$$|\psi\rangle = \sum_{n_j=0,1} \alpha_{n_1 n_2 \dots n_N} |n_1 n_2 \dots n_N\rangle, \quad (2)$$

which is expressed equivalently as

$$|\psi\rangle = \sum_{j=0}^{2^N-1} \alpha_j |j\rangle, \quad (3)$$

where j is the decimal number corresponding to the binary number $(n_1 n_2 \dots n_N)$ such as $|0\rangle = |0 \dots 00\rangle$, $|1\rangle = |0 \dots 01\rangle$, \dots , $|2^N - 1\rangle = |11 \dots 11\rangle$.

It is a key observation²⁹ that we may set

$$\alpha_j = V_j^0 e^{i\theta_j} / \sqrt{\sum_j (V_j^0)^2} \quad (4)$$

in the LC -resonator realization of quantum computation. Thus we store the information of N qubits in a set of LC resonators.

Here we propose to carry out a gate process by controlling externally the value C of a capacitance as in Fig.1(b) or the value L_1 of an inductor bridging two LC resonators as in Fig.1(c). For each gate process the initial and the final systems are the same set of 2^N identical LC resonators with the same energy, although the coefficient α_j may be modified for some j . A gate process is required to be adiabatic.

The gate U is represented by a $2^N \times 2^N$ matrix U_{jk} such that

$$U |j\rangle = \sum_{k=0}^{2^N-1} U_{jk} |k\rangle. \quad (5)$$

By this operation, the initial state ψ^{ini} is brought to the final state $\psi^{\text{fin}} = U\psi^{\text{ini}}$, where $\psi^{\text{ini}} = \sum_{j=0}^{2^N-1} \alpha_j^{\text{ini}} |j\rangle$ and $\psi^{\text{fin}} = \sum_{k=0}^{2^N-1} \alpha_k^{\text{fin}} |k\rangle$. It follows that

$$\alpha_k^{\text{fin}} = \sum_{j=0}^{2^N-1} \alpha_j^{\text{ini}} U_{jk} = \sum_{j=0}^{2^N-1} U_{kj} \alpha_j^{\text{ini}}, \quad (6)$$

since U is a symmetric matrix in universal quantum computation.

Kirchhoff law and Schrödinger equation. We first consider a set of independent LC resonators. The Kirchhoff law of the j th LC resonator may be rewritten in the form of the Schrödinger equation^{27,30},

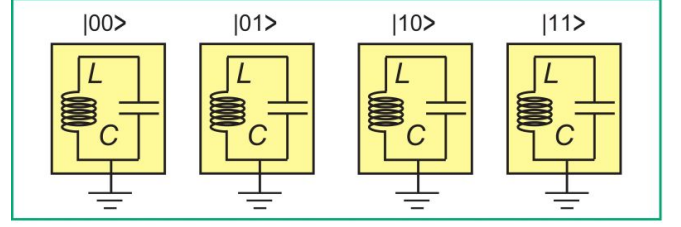
$$i \frac{d}{dt} \psi_j = H \psi_j, \quad (7)$$

where $H(t) = -\omega_0 \sigma_y$ is the Hamiltonian, and

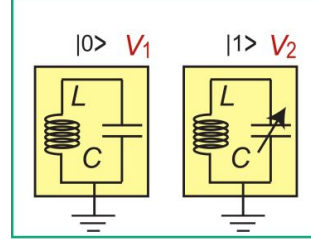
$$\psi_j = (\mathcal{I}_j, \mathcal{V}_j)^t = \left(\sqrt{L/C} I_j, V_j \right)^t \quad (8)$$

is the wave function.

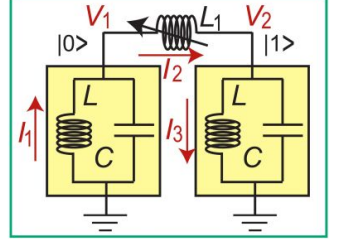
(a) Two Qubits



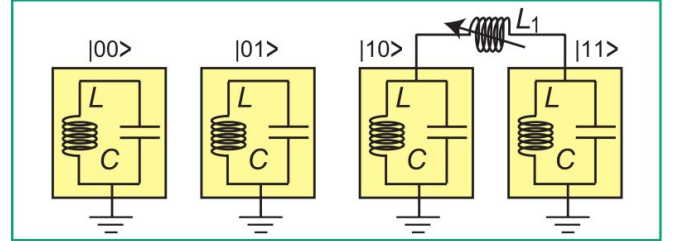
(b) Phase-shift gate



(c) Mixing gate



(d) CNOT gate



(e) Controlled phase-shift gate

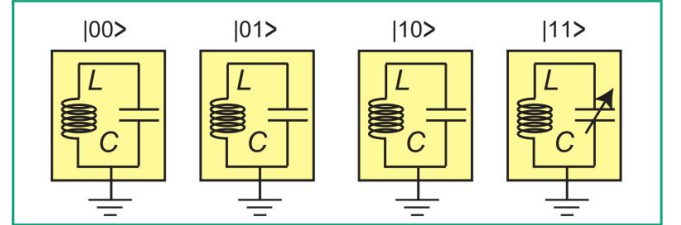


FIG. 1: (a) Two qubits made of four LC resonators. (b) Phase-shift gate consisting a pair of LC resonators. The capacitance of the state $|1\rangle$ is controlled. (c) Mixing gate. The inductance of the inductor L_1 bridging two resonators is controlled. The Hadamard gate is constructed by a combination of the mixing gate and the phase-shift gate. (d) CNOT gate. We bridge the resonators representing $|10\rangle$ and $|11\rangle$ by the inductor L_1 (e) Controlled phase-shift gate. We control the capacitance of the resonator representing $|11\rangle$.

Energy conservation and probability conservation. The total energy of the system is given by $U_T = U_E + U_M$ with

$$U_E = \frac{C}{2} \sum_j V_j^2, \quad U_M = \frac{L}{2} \sum_j I_j^2, \quad (9)$$

where U_E and U_M are the electrostatic energy and the magnetic energy, respectively.

On the other hand, by using (8), the probability of the wave

function is rewritten as

$$\sum_j |\psi_j|^2 = \sum_j \mathcal{I}_j^2 + \mathcal{V}_j^2 = \sum_j \frac{L}{C} \mathcal{I}_j^2 + \mathcal{V}_j^2 = \frac{2}{C} U_T. \quad (10)$$

Hence, the conservation of the probability of the wave function is assured by the conservation of the total energy²⁸. As we have stated, we arrange a gate process so that the total energy is the same before and after the gate process. It corresponds to the conservation of the probability for qubits $\sum_j |\alpha_j|^2 = 1$.

Phase-shift gate. The phase-shift gate is defined by the matrix

$$U_\phi = \begin{pmatrix} 1 & 0 \\ 0 & e^{i\phi} \end{pmatrix}, \quad (11)$$

which acts on the one-qubit state $(|0\rangle, |1\rangle)^t$. Namely, the action is

$$U_\phi |0\rangle = |0\rangle, \quad U_\phi |1\rangle = e^{i\phi} |1\rangle. \quad (12)$$

To generate the phase shift ϕ in the wave function, it is enough to control only the capacitance C in the LC resonator externally during the gating process as shown in Fig.1(b). We control the capacitance as $C(t) = C_0 + C_1(t)$, where

$$C_1(t) = \frac{C_1^0}{2} \left(\tanh \frac{t-t_1}{T} - \tanh \frac{t-t_2}{T} \right), \quad (13)$$

with four parameters C_1^0 , t_1 , t_2 and T , as shown in Fig.2(a1), (b1) and (c1).

It is possible to determine analytically how the phase shift ϕ depends on these parameters by calculating the Berry phase. Since the voltage evolution $V(t)$ is written as a Schrödinger equation, we may use an adiabatic approximation. The snapshot wave function at time $t = \tau$ is given by $\psi(\tau) = \sqrt{2L/C} I_0 \bar{\psi}(\tau)$, where $\bar{\psi}(\tau)$ is the normalized wave function,

$$\bar{\psi}(\tau) = \frac{1}{\sqrt{2}} \exp(i\omega_\tau \tau) \begin{pmatrix} 1 \\ -i \end{pmatrix}, \quad (14)$$

with ω_τ the snapshot frequency,

$$\omega_\tau = 1/\sqrt{LC(\tau)}. \quad (15)$$

The Berry phase is calculated as

$$\begin{aligned} \gamma &= i \int_0^t \langle \bar{\psi}(\tau) | \partial_\tau | \bar{\psi}(\tau) \rangle d\tau \\ &= \int_0^t \frac{1}{2\sqrt{LC(\tau)}^{3/2}} \left(2C(\tau) - \tau \frac{dC(\tau)}{d\tau} \right) d\tau \\ &= \int_0^t \left[\omega(\tau) - \frac{\tau}{\sqrt{LC(\tau)}^{3/2}} \frac{dC(\tau)}{d\tau} \right] d\tau. \end{aligned} \quad (16)$$

When the perturbation $C_1(t)$ is small enough with respect to C_0 , it is calculated as

$$\gamma \simeq i\omega_0 t - \phi, \quad (17)$$

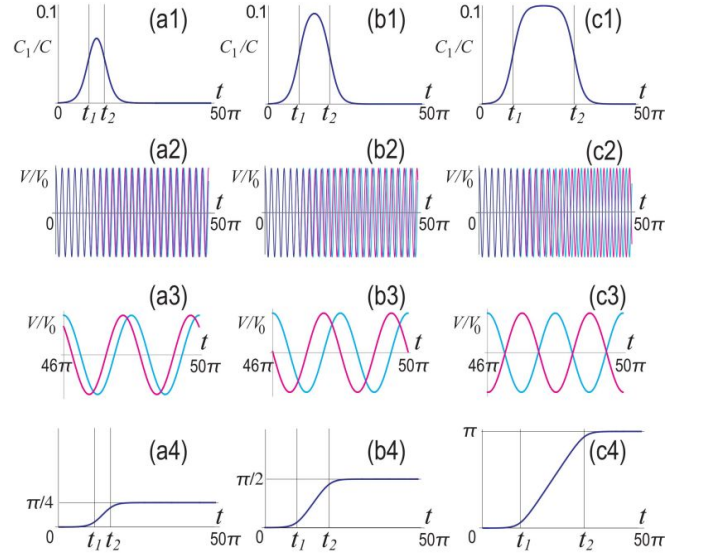


FIG. 2: Phase-shift gate for (a) $\phi = \pi/4$, (b) $\phi = \pi/2$ and (c) $\phi = \pi$. The phase delay is controlled by a time duration of the capacitance perturbation $C_1(t)$. (*1) Time evolution of the perturbed capacitance. (*2) Time evolution of the voltage V_2 . The voltage V_2 with (without) the perturbation is represented by a magenta (cyan) curve. (*3) Voltage V_2 in the final states. (*4) Phase delay as a function of time t . The horizontal axis is time t . Time span is $0 < t < 50\pi$ for (*1), (*2) and (*4). It is $46\pi < t < 50\pi$ for (*3), representing the final state. We set $C_1^0/C_0 = 0.1$ and $T = 10\omega_0$ for $0 < \omega_0 t < 50\pi$. We set $\omega_0 t_1 = 10\pi$ for all phase-shift gate. We also set $\omega_0 t_2 = 15\pi$ for the $\pi/4$ phase-shift gate, $\omega_0 t_2 = 20\pi$ for the $\pi/2$ phase-shift gate and $\omega_0 t_2 = 30\pi$ for the π phase-shift (i.e., Pauli Z) gate,

where ϕ is the phase shift given by

$$\phi = \omega_0 \int_0^t \frac{C_1(\tau)}{2C} d\tau. \quad (18)$$

It is explicitly calculated as

$$\begin{aligned} \phi &= \omega_0 \frac{C_1^0}{2C} T \left(\log \cosh \frac{t-t_1}{T} - \log \cosh \frac{t_1}{T} \right. \\ &\quad \left. - \log \cosh \frac{t-t_2}{T} + \log \cosh \frac{t_2}{T} \right), \end{aligned} \quad (19)$$

which yields

$$\phi = \frac{C_1^0 \omega_0}{2C} (t_2 - t_1), \quad (20)$$

provided $T \ll t_1 < t_2 \ll t$. Hence, we can tune the phase shift ϕ arbitrary by controlling the magnitude of $(t_2 - t_1) C_1^0$.

We next solve numerically the differential equation (7) to study the time evolution of the voltage $V(t)$, and confirm the phase-shift formula (20). When we fix $C_1^0 = 0.1C_0$ and $\omega_0 t_1 = 10\pi$, we have

$$\phi = \frac{1}{20} (\omega_0 t_2 - 10\pi). \quad (21)$$

We present numerical results of the time evolution $V(t)$ by choosing $\omega_0 t_2 = 15\pi, 20\pi$ and 30π in Fig.2(a2), (b2) and (c2). See Fig.2(a3), (b3) and (c3) for $V(t)$ for $t \gg t_2$, representing the final state. The phase shift is found to occur due to the perturbation $C_1(t)$. The phase shift $\phi(t)$ during a gating process is shown in Fig.2(a4), (b4) and (c4). After the gating process, the resonance frequency returns to ω_0 but the phase ϕ becomes different from the initial value. It reads $\phi = \pi/4, \pi/2$ and π as in Fig.2(a4), (b4) and (c4). These numerical results confirm the analytical formula (20).

Hadamard gate. The Hadamard gate is defined by the matrix

$$U_H \equiv \frac{1}{\sqrt{2}} \begin{pmatrix} 1 & 1 \\ 1 & -1 \end{pmatrix}, \quad (22)$$

which acts the one-qubit state $(|0\rangle, |1\rangle)^t$. It is known to be given by^{27,28}

$$U_H = e^{-i\pi/4} U_{\pi/2} U_{\text{mix}} U_{\pi/2}, \quad (23)$$

where $U_{\pi/2}$ is the $\pi/2$ phase-shift gate, while U_{mix} is the mixing gate defined by

$$U_{\text{mix}} = \frac{1}{\sqrt{2}} \begin{pmatrix} e^{i\pi/4} & e^{-i\pi/4} \\ e^{-i\pi/4} & e^{i\pi/4} \end{pmatrix}. \quad (24)$$

We construct the mixing gate (24) in what follows.

We consider a pair of LC resonators bridged by an inductor L_1 as shown in Fig.1(c), where the inductance L_1 is controlled externally. The Kirchhoff law reads

$$\frac{d}{dt} \begin{pmatrix} I_1 \\ I_2 \\ I_3 \\ V_1 \\ V_2 \end{pmatrix} = \begin{pmatrix} 0 & 0 & 0 & \frac{1}{L_1} & 0 \\ 0 & 0 & 0 & -\frac{1}{L_1} & \frac{1}{L_1} \\ 0 & 0 & 0 & 0 & -\frac{1}{L} \\ -\frac{1}{C} & \frac{1}{C} & 0 & 0 & 0 \\ 0 & -\frac{1}{C} & \frac{1}{C} & 0 & 0 \end{pmatrix} \begin{pmatrix} I_1 \\ I_2 \\ I_3 \\ V_1 \\ V_2 \end{pmatrix}, \quad (25)$$

where I_1, I_2, I_3, V_1 and V_2 are defined in Fig.1(c). It is rewritten in the form of the Schrödinger equation as in Eq.(7) with the Hamiltonian

$$H = \frac{1}{\sqrt{LC}} \begin{pmatrix} 0 & 0 & 0 & i & 0 \\ 0 & 0 & 0 & -iL/L_1(t) & iL/L_1(t) \\ 0 & 0 & 0 & 0 & -i \\ -i & i & 0 & 0 & 0 \\ 0 & -i & i & 0 & 0 \end{pmatrix}, \quad (26)$$

and the wave function

$$(\mathcal{I}_1, \mathcal{I}_2, \mathcal{I}_3, \mathcal{V}_1, \mathcal{V}_2) = \left(\sqrt{\frac{L}{C}} I_1, \sqrt{\frac{L}{C}} I_2, \sqrt{\frac{L}{C}} I_3, V_1, V_2 \right). \quad (27)$$

By making a snapshot approximation, the eigenvalues are given by

$$E = 0, \pm\omega_0, \pm\ell(t)\omega_0, \quad (28)$$

with

$$\ell(t) = \sqrt{1 + 2L/L_1(t)} \quad (29)$$

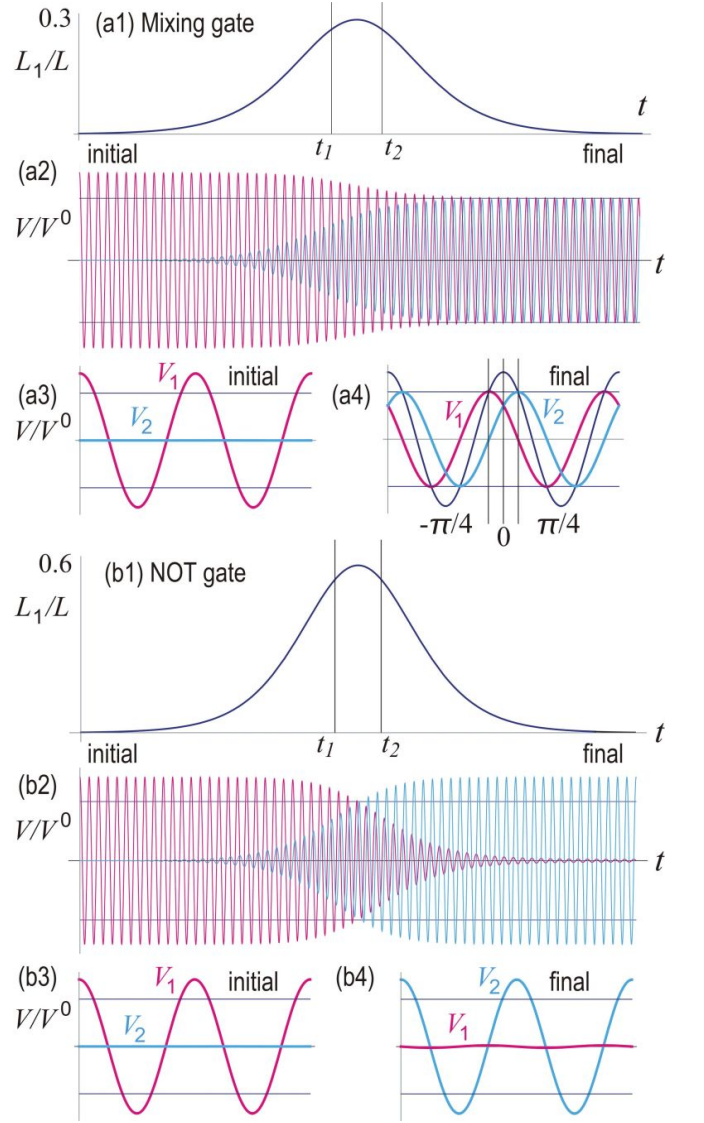


FIG. 3: (a) Mixing gate. (b) NOT gate. (a1) and (b1) Time-dependent perturbation introduced to the inductance. (a2) and (b2) Time evolution of the voltage V_1 (V_2) at the left (right) LC resonator is represented by a magenta (cyan) curve. (*3) Time evolution of V_1 and V_2 for $0 < \omega_0 t < 4\pi$, representing the initial state, where $V_2 = 0$. (*4) Time evolution V_1 and V_2 for $116\pi < t < 120\pi$, representing the final state, where the voltage without the perturbation is represented by a black curve. We set $L_1/L = 0.1$ and $T = 10\omega_0$ for $0 < \omega_0 t < 120\pi$. We set $\omega_0 t_1 = 50\pi$ and $\omega_0 t_2 = 55\pi$ for the mixing gate and $\omega_0 t_1 = 55\pi$ and $\omega_0 t_2 = 65\pi$ for the NOT gate. The orange lines represent the voltage $\pm V_0/\sqrt{2}$.

at each t .

We consider a process where the inductor L_1 is bridged to the LC resonators during a time interval $t_1 < t < t_2$ but not for $t < t_1$ and $t > t_2$. For example, we may take

$$\frac{1}{L_1(t)} = \frac{1}{2L_1} \left(\tanh \frac{t-t_1}{T} - \tanh \frac{t-t_2}{T} \right), \quad (30)$$

which we have illustrated in Fig.3(a).

We solve (25) numerically with the use of (30) and show how the voltage evolves in Fig.3. By tuning $t_2 - t_1$ and L_1 appropriately, in order to construct the mixing gate (24), we make the magnitudes of V_1 and V_2 identical in the final state, i.e., for $t \gg t_2$. We find the phase delay $\pi/4$ in V_1 and the phase advance $\pi/4$ in V_2 as in Fig.3(a4).

We may discuss the process analytically. For this purpose, we approximate (30) by a step function such that $1/L_1(t) = 0$ for $t < t_1$, $L_1(t) = L_1$ for $t_1 < t < t_2$ and $1/L_1(t) = 0$ for $t > t_2$. Two resonators are decoupled when $1/L_1(t) = 0$. For definiteness we choose $t_1 = 0$.

First, we analyze the case where only the left AC resonator is active for $t \leq 0$, or

$$V_1^{\text{ini}}(t) = V_0 \cos(\omega_0 t), \quad V_2^{\text{ini}}(0) = 0. \quad (31)$$

At $t = t_1$, the perturbation $L_1(t)$ is set on.

(i) For $0 \leq t \leq t_2$, we may solve the Kirchoff equation (25) for the voltages as

$$V_1(t) = V_0 \cos \left[\frac{\ell+1}{2} \omega_0 t \right] \cos \left[\frac{\ell-1}{2} \omega_0 t \right], \quad (32)$$

$$V_2(t) = V_0 \sin \left[\frac{\ell+1}{2} \omega_0 t \right] \sin \left[\frac{\ell-1}{2} \omega_0 t \right], \quad (33)$$

where we have chosen the initial condition to meet (31), or

$$V_1(0) = V_0, \quad V_2(0) = 0. \quad (34)$$

When $\ell \simeq 1$, the oscillation modes are made of the high-frequency mode $\frac{\ell+1}{2}\omega_0$ and the low-frequency mode $\frac{\ell-1}{2}\omega_0$.

(ii) At $t = t_2$, we require the amplitudes of $V_1(t)$ and $V_2(t)$ to be identical. Since the amplitude is determined by the low-frequency mode, the condition reads

$$\cos \left[\frac{\ell-1}{2} \omega_0 t_2 \right] = \sin \left[\frac{\ell-1}{2} \omega_0 t_2 \right] = \frac{1}{\sqrt{2}}. \quad (35)$$

Since the connection is weak, we have $L/L_1 \ll 1$, which leads to $\ell \simeq 1 + L/L_1$. We use it to derive the relation

$$\frac{L}{2L_1} \omega_0 t_2 = \frac{\pi}{4}, \quad (36)$$

which fixes t_2 to generate the mixing gate (24). The voltages read

$$V_1(t_2) = \frac{V_0}{\sqrt{2}} \cos \left[\frac{\ell+1}{2} \omega_0 t_2 \right] = \frac{V_0}{\sqrt{2}} \cos \left[\omega_0 t_2 + \frac{\pi}{4} \right], \quad (37)$$

$$V_2(t_2) = \frac{V_0}{\sqrt{2}} \sin \left[\frac{\ell+1}{2} \omega_0 t_2 \right] = \frac{V_0}{\sqrt{2}} \cos \left[\omega_0 t_2 - \frac{\pi}{4} \right], \quad (38)$$

where use was made of (32), (33) and (36). There are phase shifts $\pm \frac{\pi}{4}$.

(iii) For $t > t_2$, since the perturbation is off, two LC resonators resonate independently with the initial condition (37)

and (38), or

$$V_1^{\text{fin}}(t) = \frac{V_0}{\sqrt{2}} \cos \left[\omega_0 t + \frac{\pi}{4} \right], \quad (39)$$

$$V_2^{\text{fin}}(t) = \frac{V_0}{\sqrt{2}} \cos \left[\omega_0 t - \frac{\pi}{4} \right]. \quad (40)$$

It followed that

$$\alpha_1^{\text{ini}} = 1, \quad \alpha_2^{\text{ini}} = 0, \quad (41)$$

$$\alpha_1^{\text{fin}} = \frac{1}{\sqrt{2}} e^{i\pi/4}, \quad \alpha_2^{\text{fin}} = \frac{1}{\sqrt{2}} e^{-i\pi/4} \quad (42)$$

from Eqs.(4), (31), (39) and (40).

Next, we analyze the case where only the right AC resonator is active for $t \leq 0$, or

$$V_1^{\text{ini}}(t) = 0, \quad V_2^{\text{ini}}(0) = V_0 \cos(\omega_0 t) \quad (43)$$

instead of (31). By making precisely the same analysis, we obtain

$$\alpha_1^{\text{ini}} = 0, \quad \alpha_2^{\text{ini}} = 1, \quad (44)$$

$$\alpha_1^{\text{fin}} = \frac{1}{\sqrt{2}} e^{-i\pi/4}, \quad \alpha_2^{\text{fin}} = \frac{1}{\sqrt{2}} e^{i\pi/4}. \quad (45)$$

The results (41), (42) (44) and (45) are summarized as the mixing gate (24) based on the definition (6).

NOT gate. The NOT gate is defined by the matrix

$$U_{\text{NOT}} = \begin{pmatrix} 0 & 1 \\ 1 & 0 \end{pmatrix}, \quad (46)$$

which acts on one qubit. We find from Eq.(24) that

$$U_{\text{NOT}} = U_{\text{mix}}^2. \quad (47)$$

It is given by the sequential applications of the mixing gate. The construction is similar to that of the mixing gate provided the duration of the inductor L_1 is made twice. We present numerical results in Fig.3(b). With respect to an analytical study, the main equation is

$$\frac{L}{2L_1} \omega_0 t_2 = \frac{\pi}{2} \quad (48)$$

in place of Eq.(36).

One qubit universal gate. We may construct a combination of the Hadamard and phase-shift gates such as

$$U_{\text{1bit}} = e^{-i\theta/2} U_{\phi+\pi} U_{\text{H}} U_{\theta} U_{\text{H}} = \begin{pmatrix} \cos \frac{\theta}{2} & -i \sin \frac{\theta}{2} \\ ie^{i\phi} \sin \frac{\theta}{2} & -e^{i\phi} \cos \frac{\theta}{2} \end{pmatrix}, \quad (49)$$

which represents any SU(2) generator. It is called the one-qubit universal-quantum gate.

CNOT gate. The CNOT gate is defined by a matrix

$$U_{\text{CNOT}} = \begin{pmatrix} 1 & 0 & 0 & 0 \\ 0 & 1 & 0 & 0 \\ 0 & 0 & 0 & 1 \\ 0 & 0 & 1 & 0 \end{pmatrix}, \quad (50)$$

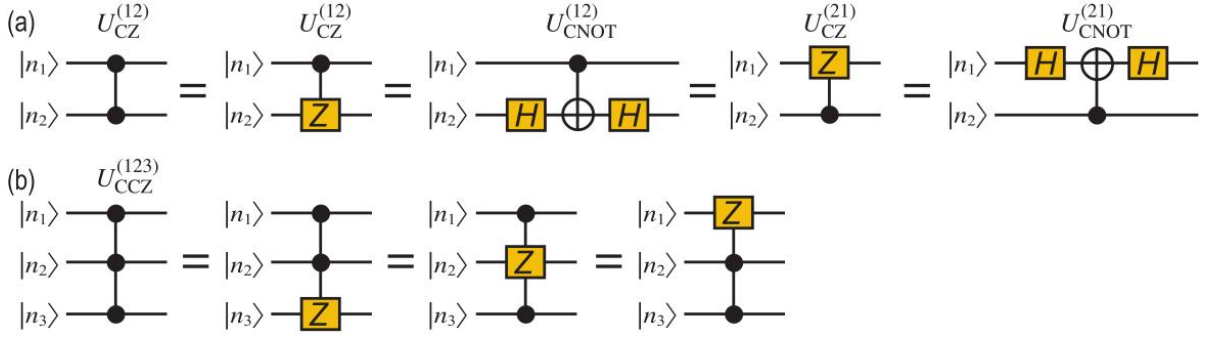


FIG. 4: Equivalent quantum-circuit representation of (a) CZ gate and (b) CCZ gate.

which acts the two-qubit state $(|00\rangle, |01\rangle, |10\rangle, |11\rangle)^t$. Two-qubit operation is constructed by using four *LC* resonators as in Fig.1. The CNOT gate is constructed by applying the NOT gate between the resonators representing $|10\rangle$ and $|11\rangle$, as shown in Fig.1(d).

Controlled Z gate. The CZ gate is defined by a matrix

$$U_{CZ} = \text{diag.} [1, 1, 1, -1], \quad (51)$$

which acts on the two-qubit state $(|00\rangle, |01\rangle, |10\rangle, |11\rangle)^t$. It follows from the definition that the controlled and target qubits are symmetric in the CZ gate, which leads to various equivalence quantum circuits as shown in Fig.4(a). We denote the CZ gate by the two black disks connected by a line.

CCZ gate. In a similar way to the CZ gate, we can construct the controlled-controlled Z (CCZ) gate acting on three qubits. It flips the sign x_7 of the state $|111\rangle$. Namely, we flip x_7 to $-x_7$. As in the case of the CZ gate, the CCZ gate is symmetric with respect to the exchange of the controlled and target qubits shown in Fig.4(b). We denote the CCZ gate by the three black disks connected by a line.

$C^{p-1}Z$ gate. We further generalize the CCZ gate to the $C^{p-1}Z$ gate. It is a p -qubit gate, which flips the sign x_{2^p-1} of the coefficient of the state $|11 \cdots 1\rangle$. As in the case of the CZ and CCZ gates, the $C^{p-1}Z$ gate is symmetric with respect to the controlled and target qubits.

More generally, we may take an N -qubit system with $N > p$. We may consider a $C^{p-1}Z$ gate acting a p -qubit subspace. We denote it by p black disks connected by a line. Such $C^{p-1}Z$ gates play an essential role to make a hypergraph state as we will soon see.

Controlled phase-shift gate. The controlled phase-shift gate is defined by the matrix

$$U_{Z_\phi} = \text{diag.} [1, 1, 1, e^{i\phi}], \quad (52)$$

which acts on two qubits. There is no action on the target qubit if the control qubit is $|0\rangle$, while the ϕ phase-shift gate is applied if the control qubit is $|1\rangle$. The controlled phase-shift gate is constructed by applying the phase-shift gate for the *LC* resonators representing $|11\rangle$, as shown in Fig.1(e).

Note that the CZ gate (51) is obtained by setting $\phi = \pi$ in the controlled phase-shift gate (52). Namely, it may be viewed as a generalization of the CZ gate, and hence we call it the CZ_ϕ gate.

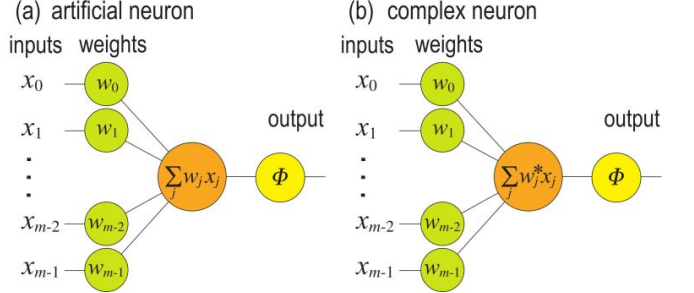


FIG. 5: (a) Schematic for an artificial neuron. It has m real inputs x_j and real internal degree of freedom named weights w_j . Output is obtained by calculating the inner product $\sum_j w_j x_j$ and then by applying an activation function $\Phi(\sum_j w_j x_j)$. (b) Schematic for a complex neuron. It has complex m inputs x_j and complex weights w_j with the inner product $\sum_j w_j^* x_j$.

$C^{p-1}Z_\phi$ gate. In a similar way to $C^{p-1}Z$ gates, we may define multi-controlled phase-shift gates, which we denote by $C^{p-1}Z_\phi$ gates. It is a p -qubit gate, which multiplies the phase $e^{i\phi}$ to the coefficient α_{2^p-1} of the state $|11 \cdots 1\rangle$.

III. ARTIFICIAL NEURON

An artificial neuron is a mathematical model^{43,44} to simulate a biological neuron. There are m inputs x_0, x_1, \dots, x_{m-1} and m weights w_0, w_1, \dots, w_{m-1} , where, x_j and w_j are real numbers. We represent the input and the weight by wave functions as⁴⁸

$$|\psi_x\rangle = \frac{1}{\sqrt{2^N}} \sum_{j=0}^{2^N-1} x_j |j\rangle, \quad |\psi_w\rangle = \frac{1}{\sqrt{2^N}} \sum_{j=0}^{2^N-1} w_j |j\rangle, \quad (53)$$

where $|j\rangle$ forms the N qubit basis as in Eq.(3). Note the difference between the coefficients α_j in Eq.(3) and x_j, w_j in Eq.(53) by the factor $1/\sqrt{2^N}$.

The first step in the artificial neuron is to calculate the inner product $\sum_j w_j x_j$. The inner product of the input data and the weight data measures the similarity between them. For instance, using a series of numbers representing a set of ref-

(a) 5 × 4 pixels				(b) 6 × 5 pixels				
00000	00001	00010	00011	00000	00001	00010	00011	00100
00100	00101	00110	00111	00101	00110	00111	01000	01001
01000	01001	01010	01011	01010	01011	01100	01101	01110
01100	01101	01110	01111	01111	10000	10001	10010	10011
10000	10001	10010	10011	10100	10101	10110	10111	11000
				11001	11010	11011	11100	11101

FIG. 6: Assignment of binary numbers to (a) 5 × 4 pixels for the number recognition and (b) 6 × 5 pixels for the alphabet recognition.

erence patterns as the weight, we may calculate the similarity between an input pattern and the reference pattern.

The inner product is outputted after applying an activation function,

$$y = \Phi\left(\sum_j w_j x_j\right). \quad (54)$$

The activation function Φ has various forms such as the step function^{56,57}, a linear function, a sigmoid function, a ramp function⁵⁸ and so on. We show a schematic of a neuron in Fig.5(a). In the process of artificial neuron, the heaviest procedure is the calculation of $\sum_j w_j x_j$, which is efficiently done by using a quantum computer⁴⁸.

We implement the wave functions (53) by unitary transformations from the initial state $|0\rangle$,

$$|\psi_x\rangle = U_x |0\rangle, \quad |\psi_w\rangle = U_w^\dagger |0\rangle. \quad (55)$$

Then, the inner product is calculated as

$$\sum_j w_j x_j = 2^N \langle \psi_w | \psi_x \rangle = 2^N \langle\langle 0 | U_w U_x | 0 \rangle\rangle. \quad (56)$$

We explicitly construct U_x and U_w later in this section. On the other hand, the application of Φ is easy with the use of a classical computer since it is a one-to-one map.

A simplest artificial neuron is given by the perceptron model^{56,57}. Here, the input and the weight wave functions are given by Eq.(53) with $x_j = \pm 1$ and $w_j = \pm 1$. Such states are called real equally weighted (REW) states. Furthermore, the step function is used as the activation function,

$$y = \Theta\left(\sum_j w_j x_j - h\right), \quad (57)$$

where Θ is a step function with the threshold h , $\Theta(x - h) = 1$ for $x \geq h$ and $\Theta(x - h) = -1$ for $x < h$.

In our application of artificial neuron to pattern recognition we use REW states as in the perceptron model but without employing the activation function (57). We use the inner product itself as the output.

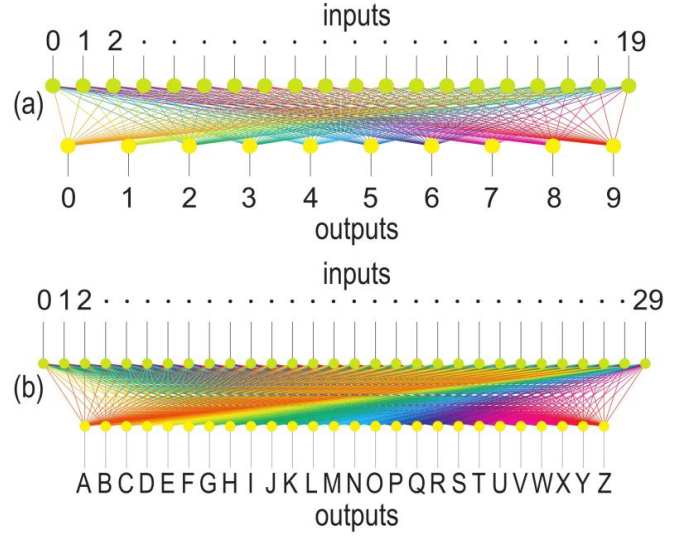


FIG. 7: Neural networks for (a) number recognition and (b) alphabet recognition.

We now discuss how to construct a REW state from the initial state $|0\rangle$, or how to determine U_x and U_w^\dagger in Eq.(55) in the standard quantum-circuit implementation⁴⁸ and also in the electric-circuit implementation.

In the first step, we prepare the equal-coefficient state defined by

$$|\psi_0\rangle = \frac{1}{\sqrt{2^N}} \sum_{j=0}^{2^N-1} |j\rangle \equiv \frac{1}{\sqrt{2^N}} \sum_{n_j=0,1} |n_1 n_2 \cdots n_N\rangle. \quad (58)$$

This is done by way of the Walsh-Hadamard transform of the initial state $|0\rangle$,

$$|\psi_0\rangle = \bigotimes_{s=1}^N U_H^{(s)} |0\rangle, \quad (59)$$

where $U_H^{(s)}$ is the Hadamard gate acting on the s th qubit.

In the second step, we construct $|\psi_x\rangle$ and $|\psi_w\rangle$ from the equal-coefficient state as

$$|\psi_x\rangle = V_x |\psi_0\rangle, \quad |\psi_w\rangle = V_w^\dagger |\psi_0\rangle. \quad (60)$$

Here, V_x is an operation by changing the coefficient x_j in the state $|\psi_x\rangle$ to $-x_j$ if $x_j = -1$ for all j . Hence, V_x is given by a sequential application of $C^{p-1}Z$ gates. For this purpose, we search for the qubit state $|j\rangle$ whose coefficient is $x_j = -1$. Then, we apply an appropriate $C^{p-1}Z$ gate to the state to change its coefficient to $x_j = 1$. An explicit example is given in Appendix A.

We find from (55), (59) and (60) that

$$U_x = V_x \bigotimes_{s=1}^N U_H^{(s)}, \quad U_w^\dagger = V_w^\dagger \bigotimes_{s=1}^N U_H^{(s)}, \quad (61)$$

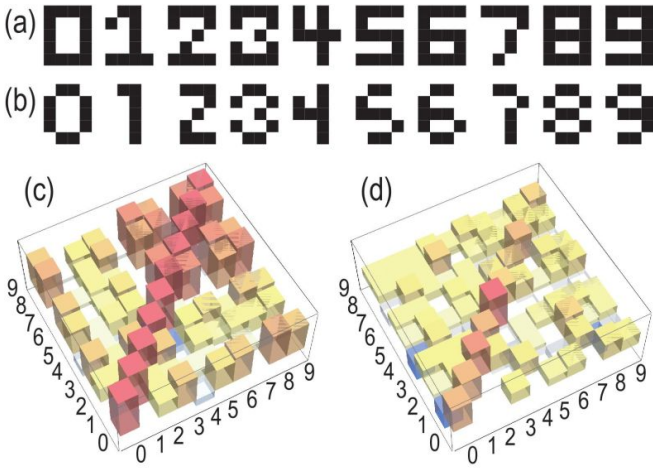


FIG. 8: (a) Reference patterns and (b) input patterns of numbers. (c) Self similarity $\langle \psi_w | \psi_w \rangle$ and (d) cross similarity $\langle \psi_w | \psi_x \rangle$ of the number recognition.

and from (56) and (61) that

$$\sum_j w_j x_j = 2^N \langle \psi_w | \psi_x \rangle = 2^N \langle \langle 0 | \bigotimes_{s=1}^N U_H^{(s)} V_w V_x \bigotimes_{s=1}^N U_H^{(s)} | 0 \rangle \rangle. \quad (62)$$

This is the basic formula to calculate the inner product by a quantum computer starting from the initial state $|0\rangle$. An explicit example of implementation is given in Sec.VII

IV. PATTERN RECOGNITION

Pattern recognition is one of the most useful applications of artificial neurons. As an example, we consider a pattern made of rectangular pixels painted in black and white. We show two patterns made of 5×4 pixels and 6×5 pixels, which are labelled by binary codes as in Fig.6(a) and (b). Next, we assign $x_j = 1$ for white pixel and $x_j = -1$ for black pixel. Here, j is a decimal number representing a binary code assigned to a pixel, $0 \leq j \leq N_p - 1$.

In order to represent $N_x \times N_y$ pixels, we prepare N qubits satisfying $2^{N-1} < N_x \times N_y \leq 2^N$. These N -qubit states are REW states, which are Eq.(53) with $x_j = \pm 1$ and $w_j = \pm 1$. Let there be N_p patterns to be classified. It is $N_p = 10$ for the number recognition and $N_p = 26$ for the alphabet recognition as in Fig.7(a) and (b), respectively. We use a set of reference patterns as the weight wave function $|\psi_w(j)\rangle$, and compare them with a set of input patterns $|\psi_x(j)\rangle$: Examples are given in Fig.8 for $N_p = 10$ and in Fig.9 for $N_p = 26$. In these cases, it is enough to prepare five qubits. We estimate the similarity between an input pattern and the reference pattern by calculating the inner product $\langle \psi_w | \psi_x \rangle$. We determine which input pattern is most similar to the reference pattern by searching the largest inner product $\langle \psi_w | \psi_x \rangle$. This process is expressed by a single layer neural network with $N_x \times N_y$ inputs and N_p

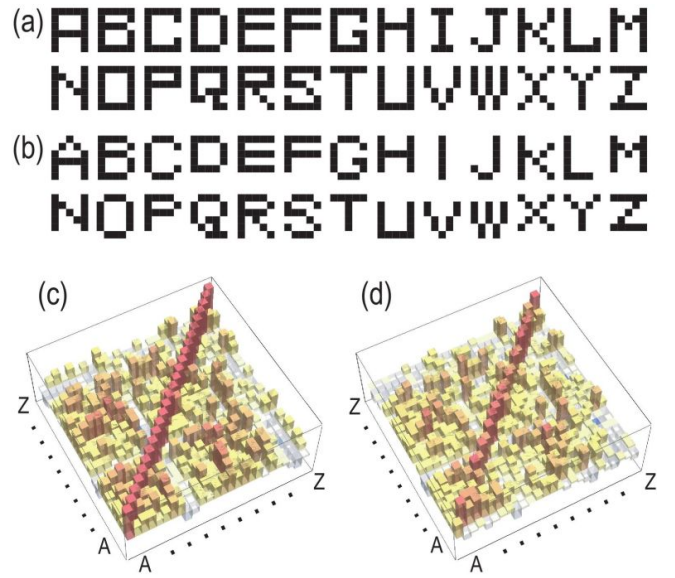


FIG. 9: (a) Reference patterns and (b) input patterns of alphabets. (c) Self similarity $\langle \psi_w | \psi_w \rangle$ and (d) cross similarity $\langle \psi_w | \psi_x \rangle$ of the alphabet recognition.

outputs as in Fig.7. The inner product is calculated as

$$\langle \psi_w | \psi_x \rangle = \frac{N_p - 2N_{\text{error}}}{N_p}, \quad (63)$$

where N_{error} is the number of errors between the reference and the input patterns defined by

$$N_{\text{error}} = \sum_{j=0}^{N_p-1} \left(\frac{x_j - w_j}{2} \right)^2. \quad (64)$$

We note that $\langle \psi_w | \psi_x \rangle$ can be negative for $N_{\text{error}} \geq N_p/2$. We find $|\langle \psi_w | \psi_x \rangle| \leq 1$, where $\langle \psi_w | \psi_x \rangle = 1$ indicates the perfect matching.

As the first example, we study a recognition of numbers. We choose a set of the reference patterns of numbers as given by Fig.8(a). We implement them into a wave function $|\psi_w\rangle$. Explicit forms are shown in Appendix B. Then, we take a set of input patterns. See Fig.8(b) for an instance. First, we calculate the self similarity defined by $\langle \psi_w(j_1) | \psi_w(j_2) \rangle$, which is shown in Fig.8(c). The maximum values are taken when $j = j_1 = j_2$ with $\langle \psi_w(j) | \psi_w(j) \rangle = 1$. In order to well recognize different patterns as different ones, it is necessary that $\langle \psi_w(j_1) | \psi_w(j_2) \rangle$ is small for $j_1 \neq j_2$. From Fig.8(c), we find that 1, 2, 3, 4, 5 and 7 are well distinguishable because $\langle \psi_w(j_1) | \psi_w(j_2) \rangle$ is low. On the other hand, 6, 8 and 9 are hardly distinguishable because the similarity is 0.9, where only one pixel is different.

Next, we study a cross similarity between the input and the reference patterns by calculating $\langle \psi_w(j_1) | \psi_x(j_2) \rangle$. We fix j_2 for the input pattern and determine which reference pattern is most similar by choosing the largest inner product. We find 0, 1, 2, 3, 4, 5, 6, 7 and 9 are correctly recognized, but 8 is ill recognized to be 3. See Fig.8(d).

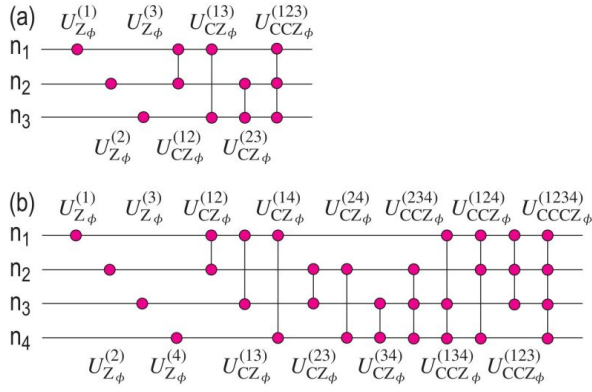


FIG. 10: Standard quantum circuits for a generation process of the CEW state for (a) three qubits and (b) four qubits. An isolated magenta disk indicates a Z gate. Magenta disks connected by a line indicate a $C^{p-1}Z_\phi$ gate.

In a similar way, we study an alphabet recognition. We choose a set of the reference patterns of alphabets as in Fig.9(a) and a set of input patterns in Fig.9(b). The self-similarity and the cross-similarity are shown in Fig.9(c) and (d). We find the following properties from the self similarity: Alphabets are easier to differentiate comparing to numbers. "F" is hardly differentiated from "P", where the similarity is 14/15. "C", "D", "G" and "O" are hardly differentiable among themselves, and "M" and "N" are hardly differentiated one another, where the similarity is 13/15. We find the following properties from the cross similarity: There are ill recognitions of "D" to "Q", "E" to "F", "O" to "D", "X" to "Y" and "Z" to "T". In addition, "C" has equal similarity to both "C" and "D" in the reference pattern, "G" has equal similarity to both "D" and "G". "I" has equal similarity to both "I" and "T". For other cases, the input patterns are well recognized with respect to the reference patterns.

V. COMPLEX-ARTIFICIAL NEURON

We proceed to study a complex-artificial neuron, where the input and the weight are given by CEW states. Namely, the wave functions are given by (53) with complex coefficients $x_j = e^{i\theta_j^x}$ and $w_j = e^{i\theta_j^w}$. The inner product reads

$$\langle \psi_w | \psi_x \rangle = \frac{1}{2^N} \sum_j w_j^* x_j = \frac{1}{2^N} \sum_j e^{i(\theta_j^x - \theta_j^w)}. \quad (65)$$

The output is given by⁵²

$$y = \Phi\left(\sum_j w_j^* x_j\right), \quad (66)$$

where Φ is a complex-activation function.

Any CEW state is generated by a sequential application of $C^{p-1}Z_\phi$ gates to the equal-coefficient state (58) precisely as the REW state is generated by a sequential application of $C^{p-1}Z$ gates to it. Let us explain it by taking the most general



FIG. 11: (a) Color circle, (b) reference color pattern and (c) input color pattern. The input pattern is made by changing randomly colors of the reference pattern within 20% randomness.

CEW state $|\psi\rangle$ in the 3-qubit system. It is given by

$$|\psi\rangle = \sum_{n_j=0,1} \alpha_{n_1 n_2 n_3} |n_1 n_2 n_3\rangle, \quad (67)$$

with

$$\alpha_{n_1 n_2 n_3} = \frac{1}{\sqrt{2^N}} \exp(i\theta_{n_1 n_2 n_3}), \quad (68)$$

where we set $\theta_{000} = 0$ without loss of generality.

We list up all possible $C^{p-1}Z_\phi$ gates in Fig.10(a). Recall that all $C^{p-1}Z_\phi$ gates are commutative. The generated CEW state is given by

$$\begin{aligned} & U_{CCZ_{\phi_{123}}}^{(123)} U_{CZ_{\phi_{23}}}^{(23)} U_{CZ_{\phi_{13}}}^{(13)} U_{CZ_{\phi_{12}}}^{(12)} U_{Z_{\phi_3}}^{(3)} U_{Z_{\phi_2}}^{(2)} U_{Z_{\phi_1}}^{(1)} \bigotimes_{s=1}^4 U_H^{(s)} |0\rangle \\ &= \frac{1}{\sqrt{8}} (|000\rangle + e^{i\phi_3} |001\rangle + e^{i\phi_2} |010\rangle + e^{i(\phi_2+\phi_3+\phi_{23})} |011\rangle \\ &\quad + e^{i\phi_1} |100\rangle + e^{i(\phi_1+\phi_3+\phi_{13})} |101\rangle + e^{i(\phi_1+\phi_2+\phi_{12})} |110\rangle \\ &\quad + e^{i(\phi_1+\phi_2+\phi_3+\phi_{12}+\phi_{13}+\phi_{23}+\phi_{123})} |111\rangle), \end{aligned} \quad (69)$$

where the angle ϕ_1 is that of the Z_{ϕ_1} gate, ϕ_{12} is that of $CZ_{\phi_{12}}$ and ϕ_{123} is that of $CCZ_{\phi_{123}}$, and so on.

It is easy to see that the angles associated with $C^{p-1}Z_\phi$ gates (69) are uniquely fixed in terms of $\theta_{n_1 n_2 n_3}$ in the given CEW state (67) because there are seven independent variables in both of these equations. Indeed, by equating (67) and (69), we obtain relations

$$\begin{aligned} \phi_1 &= \theta_{100}, & \phi_2 &= \theta_{010}, & \phi_3 &= \theta_{001}, \\ \phi_{12} &= \theta_{110} - \theta_{100} - \theta_{010}, \\ \phi_{13} &= \theta_{101} - \theta_{100} - \theta_{001}, \\ \phi_{23} &= \theta_{011} - \theta_{010} - \theta_{001}, \\ \phi_{123} &= \theta_{111} + \theta_{100} + \theta_{010} + \theta_{001} - \theta_{110} - \theta_{101} - \theta_{011}. \end{aligned} \quad (70)$$

We have shown which $C^{p-1}Z_\phi$ gates we have to prepare in order to generate the most general CEW state (67) in the 3-qubit system.

We also list up all possible $C^{p-1}Z_\phi$ gates for the 4-qubit system in Fig.10(b). In general, we can always construct an arbitrary CEW state by applying $C^{p-1}Z_\phi$ gates in N -qubit systems.

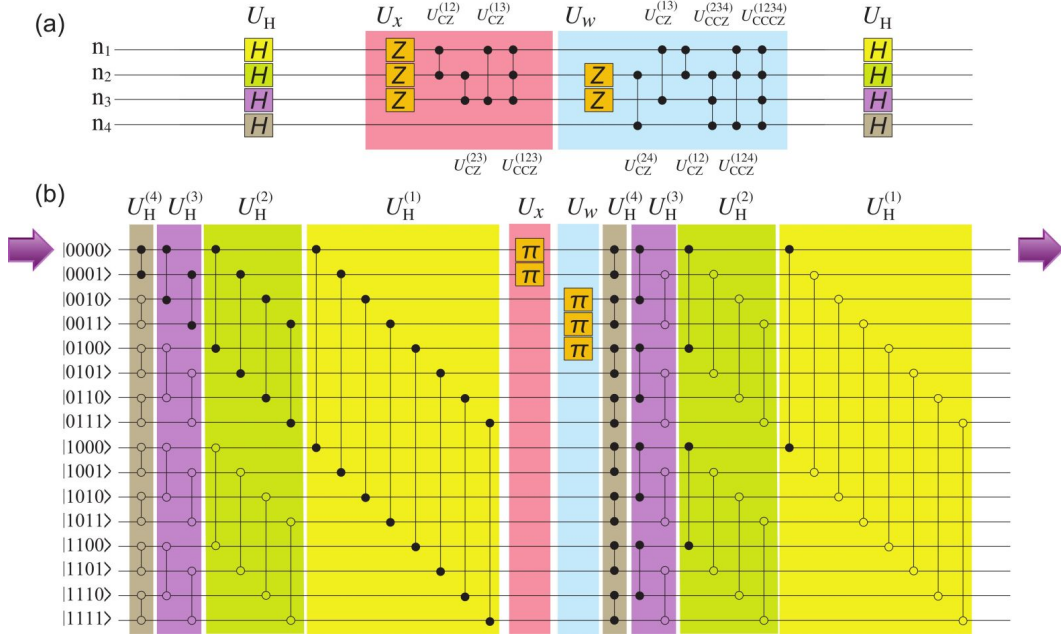


FIG. 12: (a) Standard quantum-circuit model for the calculation of the inner product (71) for an example given by (74) and (75). We use a four-qubit state $|n_1 n_2 n_3 n_4\rangle$ (b) Corresponding electric-circuit simulation. The Hadamard gates are denoted by filled or unfilled black disks connected by a link. The Hadamard bridges with unfilled disks are not necessary since they are irrelevant for the input state $|0\rangle$ and the output state $\langle 0|$.

VI. COLORED PATTERN RECOGNITION

The color circle is a color pallet indexed by a number on a circle as shown in Fig.11(a). It has a one-to-one correspondence to $e^{i\theta}$. For example, $\theta = 0$ indicates red and $\theta = \pi$ indicates cyan. Hence, a color pattern made of pixels is well represented by a CEW state. By using a complex neural network, we can estimate a similarity between two colored patterns.

For example, we show a reference colored pattern in Fig.11(b). It is enough to prepare 4 qubits for a pattern with 16 pixels. We make an input colored pattern by modifying color randomly within 20%. The inner product of two patterns is $0.993 - 0.096i$. It is relatively large although the color of each pixel is modified by 20%. This is because the input pattern is created from the reference pattern by adding noise, where the noise is cancelled by adding all contributions from pixels. Hence, our scheme can evaluate similarity between two colored patterns with color noise.

The merit of our color representation scheme is that the color circle is naturally represented by a continuous circle $e^{i\theta}$. In the standard digital representation, we have to digitalize color. The number of classical bits increases as the increase of hue decomposition. On the other hand, all color is continuously represented by one number $e^{i\theta}$ in our scheme.

VII. ELECTRIC-CIRCUIT IMPLEMENTATION

We implement these models by a set of LC resonators. We prepare 2^N LC resonators to represent the states $|j\rangle$ or $|n_1 n_2 \cdots n_s \cdots n_N\rangle$. The main issue is the electric-circuit implementation of the inner product formula (62), or

$$\langle \psi_w | \psi_x \rangle = \langle\langle 0 | \bigotimes_{s=1}^N U_H^{(s)} V_w V_x \bigotimes_{s=1}^N U_H^{(s)} | 0 \rangle\rangle, \quad (71)$$

which may be used for CEW states as well as REW states.

The first step is the construction of the equal-coefficient state (58) by applying $\bigotimes_{s=1}^N U_H^{(s)}$ to the initial state $|0\rangle$. The action of the Hadamard transformation $U_H^{(s)}$ for the s th qubit is simulated by bridging two resonators $|n_1 n_2 \cdots n_s \cdots n_N\rangle$ and $|n_1 n_2 \cdots \bar{n}_s \cdots n_N\rangle$, when $\bar{n}_s = 1$ for $n_s = 0$ and $\bar{n}_s = 0$ for $n_s = 1$. In the case of $N = 4$, the Hadamard gate $U_H^{(1)}$ is simulated by the eight bridges between

$$\begin{array}{ll} |0000\rangle & \text{and} & |1000\rangle, \\ |0001\rangle & \text{and} & |1001\rangle, \\ |0010\rangle & \text{and} & |1010\rangle, \\ |0011\rangle & \text{and} & |1011\rangle, \\ |0100\rangle & \text{and} & |1100\rangle, \\ |0101\rangle & \text{and} & |1101\rangle, \\ |0110\rangle & \text{and} & |1110\rangle, \\ |0111\rangle & \text{and} & |1111\rangle. \end{array} \quad (72)$$

Although there are many bridges, their assignment is systematic. Apparently we need $N2^{N-1}$ operations. Actually, many

bridges shown by unfilled disks in Fig.12(b) are not necessary since we start with $|0\rangle\rangle$ and end up with $\langle\langle 0|$ as in Eq.(71). Then, we may delete all operations which is irrelevant to the input and the output, which greatly reduces the number of operations. The necessary operation relating to the N -qubit Hadamard gate is $\sum_s^N 2^{s-1} = 2^N - 1$. The reduction rate is

$$\lim_{N \rightarrow \infty} \frac{2^N - 1}{N2^{N-1}} = \lim_{N \rightarrow \infty} \frac{2}{N}. \quad (73)$$

The second step is the operation of $C^{p-1}Z$ gates in the case of REW states. In construct to the application of $C^{p-1}Z$ gates in the standard quantum-circuit implementation, it is enough to apply the π phase-shift only for $|j\rangle\rangle$ with $x_j = -1$. More explicitly, the CZ gate for two qubits is simulated by the π phase-shift gate applied to the resonator representing $|11\rangle$, while the CCZ gate for three qubits is simulated by the π phase-shift gate applied to the resonator representing $|111\rangle$. In general, the $C^{p-1}Z$ gate for p qubits is simulated by the π phase-shift gate applied only to the resonator representing $|11 \dots 1\rangle$.

We consider an example of an inner product for the input and the weight states given by

$$\begin{aligned} 4|\psi_x\rangle = & -|0000\rangle - |0001\rangle + |0010\rangle + |0011\rangle \\ & + |0100\rangle + |0101\rangle + |0110\rangle + |0111\rangle \\ & + |1000\rangle + |1001\rangle + |1010\rangle + |1011\rangle \\ & + |1100\rangle + |1101\rangle + |1110\rangle + |1111\rangle, \end{aligned} \quad (74)$$

and

$$\begin{aligned} 4|\psi_w\rangle = & |0000\rangle + |0001\rangle - |0010\rangle - |0011\rangle \\ & - |0100\rangle + |0101\rangle + |0110\rangle + |0111\rangle \\ & + |1000\rangle + |1001\rangle + |1010\rangle + |1011\rangle \\ & + |1100\rangle + |1101\rangle + |1110\rangle + |1111\rangle, \end{aligned} \quad (75)$$

where the inner product is $\langle\psi_w|\psi_x\rangle = 3/8$. The quantum circuit and the electric circuit to calculate this inner product based on the inner product formula (62) are given in Fig.12(a). Then, we apply the π phase-shift gate for $|0000\rangle$ and $|0001\rangle$ in order to construct $|\psi_x\rangle$, while we apply the π phase-shift gate for $|0010\rangle$, $|0011\rangle$ and $|0100\rangle$ in order to construct $|\psi_w\rangle$ as in Fig.12(b).

It is convenient to define the output y_j for each resonator representing $|j\rangle\rangle$ in Fig.13 by

$$\frac{1}{4} \sum_{j=0}^{15} y_j |j\rangle\rangle = \left(\bigotimes_{s=1}^4 U_H^{(s)} \right) V_w V_x \left(\bigotimes_{s=1}^4 U_H^{(s)} \right) |0000\rangle. \quad (76)$$

The outs y_j are always real. Especially, we are interested in the output for $|0000\rangle$, which is $y_0 = 3/8$. It reproduce a correct the inner product given below Eq.(75).

The generalization to the calculation of an inner product of CEW states is straightforward. As a characteristic feature of the present electric-circuit simulation, it is possible to create a ϕ phase-shift gate with an arbitrary angle ϕ just by tuning the capacitance of the relevant LC resonator according the formula (20). Hence, any CEW state is generated by applying $C^{p-1}Z_\phi$ gates with the use of appropriate ϕ phase-shift gates.

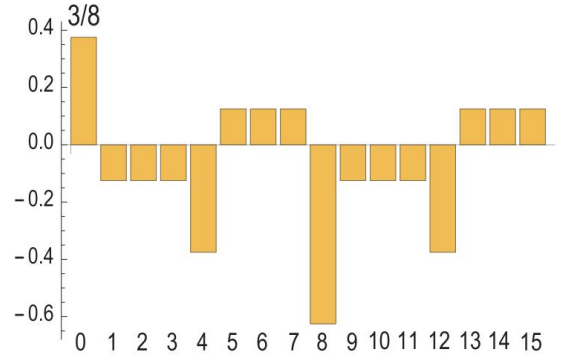


FIG. 13: Output y_j for each resonator representing $|j\rangle\rangle$. We measure the output y_0 for the state $|0\rangle\rangle$, which gives an inner product $3/8 = 0.375$.

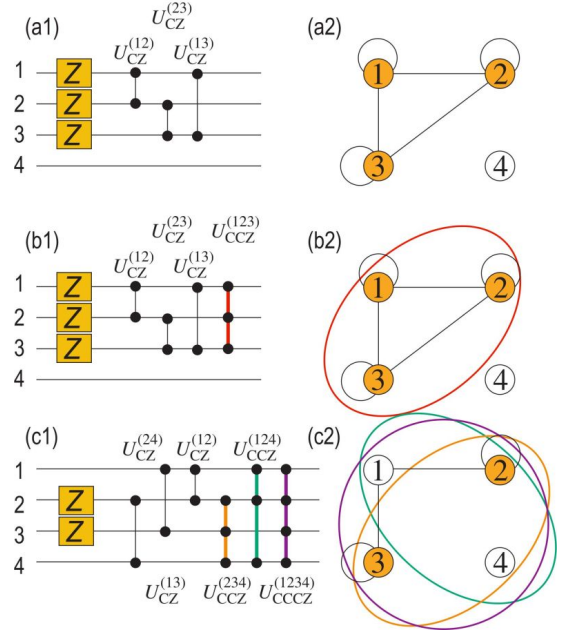


FIG. 14: (*1) Quantum-circuit representation, and (*2) graph and hypergraph representation. Z gates correspond to self-loops, which are marked in orange disks in a graph or a hypergraph. CZ gates correspond to edges, which are marked in black lines in a hypergraph. $C^{p-1}Z$ gates correspond to hyperedges, which are marked in colored ovals in a hypergraph. (a*) graph state, (b*) for ψ_x and (c*) for ψ_w .

VIII. GRAPH THEORY

Graph states and hypergraph states. It is intriguing to examine the REW state in the context of graph theory. Such a state is referred to as a graph state⁵⁹⁻⁶¹ that is constructed by a sequential application of Z gates and CZ gates to the equal-coefficient state (58). The order of a Z gate and a CZ gate is irrelevant because they are diagonal operators and commutable. Then, we may establish one-to-one correspondence between a graph and a graph state. Indeed, in order to make a graph corresponding to a graph state, we first prepare N vertices representing N qubits, as in Fig.14(a2) for an instance

of $N = 4$. We add self-loop links to the vertices to which Z gates are applied, while we connect two vertices by an edge where CZ gates are operated. Different graphs represent different graph states due to the commutative nature of the Z and the CZ gates. See Fig.14(a2).

The set of all graph states is a subgroup of the REW states by the following reasoning. The number of the Z gates is N , while the number of the CZ gates is ${}_N C_2$. Hence, we can express $2^{N+{}_N C_2}$ graph states. On the other hand, the number of the REW states is 2^{2^N} . Here, $2^{2^N} > 2^{N+{}_N C_2}$ for $N \geq 3$.

In order to represent a complete set of the REW states, it is necessary to introduce the notion of hypergraph^{55,62}, which is a generalization of graph. In a hypergraph, we have a hyperedge connecting more than three vertices. For example, a CCZ gate is represented by a hyperedge with order 3, which connects three vertices, as in Fig.14(b2). In a similar way, a $C^{p-1}Z$ gate is represented by a hyperedge with order p , which connects p vertices. The number of the $C^{p-1}Z$ gates is given by ${}_N C_p$. Then, the total number of gates is $2^{\sum_{p=1}^N ({}_N C_p)} = 2^{2^N - 1}$. The overall phase is irrelevant and thus it is a complete representation. We show a hypergraph representation of $|\psi_x\rangle$ and $|\psi_w\rangle$ in Fig.14. In Fig.14(b), a hyperedge is represented by an oval containing three vertices connected by a hyperedge. In Fig.14(c), three hyperedges are represented by three ovals containing vertices connected by three hyperedge.

Weighted graph states and hypergraph states. As a generalization of graph states and hypergraph states, we may introduce the concepts of weighted graph states and weighted hypergraph states in the context of CEW states. A weighted graph state is defined by a sequential application of Z_ϕ gates and CZ_ϕ gates to the equal-coefficient state (58), where $e^{i\phi}$ is a weight. Next, a weighted hypergraph state is generated by a sequential application of $C^{p-1}Z_\phi$ gates to the equal-coefficient state (58). Here, we assign a p -hyperedge to a $C^{p-1}Z_\phi$ gate as in the case of $C^{p-1}Z$ gates, and then we assign a weight $e^{i\phi}$ to each hyperedge.

IX. DISCUSSION

We have proposed an electric-circuit simulation of universal quantum gates on the basis of LC resonators bridged by inductors. Here, capacitance and inductance are controllable by using a variable capacitance diode and an active inductor,

respectively.

An artificial neuron requires many $C^{p-1}Z$ gates for various p . It is actually a hard task to realize $C^{p-1}Z$ gates in the standard quantum-circuit implementation even by employing modern technology such as superconductor, ion-trap or photonic systems for $p \geq 3$. This difficulty originates in the fact that a $C^{p-1}Z$ gate implies a p -body interaction. Although it is possible to decompose a $C^{p-1}Z$ gate into simpler gates, there emerge many gates³. The problem becomes worse for a complex-artificial neuron, where we use $C^{p-1}Z_\phi$ gates instead of $C^{p-1}Z$ gates. The $C^{p-1}Z_\phi$ gate contains the phase-shift gate with angle ϕ . It is possible but quite tedious to construct a $C^{p-1}Z_\phi$ gate with the use of a set of universal quantum gates. On the contrary, it is simple to construct a $C^{p-1}Z_\phi$ gate by inserting one ϕ phase-shift gate in the electric-circuit implementation.

Furthermore, it is a nontrivial problem to construct a superposition state such as REW or CEW states. It is necessary to design several quantum gates in order to make such a state, for which we need to use a classical computer in general. See a typical example in Fig.12(a) and Appendix A. On the other hand, it is sufficient to insert simply some ϕ phase-shift gates in the electric-circuit implementation. Although the implementation of the Hadamard gates is harder, the assignment is systematic and trivial. See the corresponding example in Fig.12(b).

We have previously proposed another kind of electric-circuit simulation of universal quantum gates, where quantum gates are constructed by bridging telegrapher wires^{27,28}. The number of elements of electric circuits increases as the increase of the number of quantum gates. On the other hand, the number of the elements is fixed in the present scheme irrespective to the number of quantum gates because the operation is performed in time evolution. Another merit comparing to the wire construction is that the present scheme is programmable because the gate is applied temporally, which is contrasted to the wire construction where the gates are constructed by setting wires.

The author is very much grateful to E. Saito and N. Nagaosa for helpful discussions on the subject. This work is supported by the Grants-in-Aid for Scientific Research from MEXT KAKENHI (Grants No. JP17K05490 and No. JP18H03676). This work is also supported by CREST, JST (JPMJCR16F1 and JPMJCR20T2).

Appendix A: Example of hypergraph generation process

A REW state $|\psi_x\rangle$ is given by Eq.(53) with $x_j = \pm 1$. We explain how to create this state from the equal-coefficient state (58). Alternatively, we explain how to transform this state to the equal-coefficient state.

Let us explicitly study an example given by

$$4|\psi_x\rangle = -|0000\rangle - |0001\rangle + |0010\rangle + |0011\rangle + |0100\rangle + |0101\rangle + |0110\rangle + |0111\rangle + |1000\rangle + |1001\rangle + |1010\rangle + |1011\rangle + |1100\rangle + |1101\rangle + |1110\rangle + |1111\rangle. \quad (\text{A1})$$

First, we rewrite it so that the coefficient of $|0000\rangle$ is 1,

$$4|\psi_x\rangle = -(|0000\rangle + |0001\rangle - |0010\rangle - |0011\rangle - |0100\rangle - |0101\rangle - |0110\rangle - |0111\rangle - |1000\rangle - |1001\rangle - |1010\rangle - |1011\rangle - |1100\rangle - |1101\rangle - |1110\rangle - |1111\rangle). \quad (\text{A2})$$

We note that overall phase $-$ is irrelevant in quantum computation.

(i) We focus on the states $|n_1n_2n_3n_4\rangle$ such that $\sum_i n_i = 1$, among which the coefficients of $|1000\rangle$, $|0100\rangle$ and $|0010\rangle$ are -1 , while the coefficient of $|0001\rangle$ is 1. Then, we apply three Z gates to the first, second and third qubits, and obtain

$$4U_Z^{(1)}U_Z^{(2)}U_Z^{(3)}\psi_x = -(|0000\rangle + |0001\rangle + |0010\rangle + |0011\rangle + |0100\rangle + |0101\rangle - |0110\rangle - |0111\rangle + |1000\rangle + |1001\rangle - |1010\rangle - |1011\rangle - |1100\rangle - |1101\rangle + |1110\rangle + |1111\rangle) \quad (\text{A3})$$

(ii) We focus on the states $|n_1n_2n_3n_4\rangle$ such that $\sum_i n_i = 2$, among which the coefficients of $|0110\rangle$, $|1010\rangle$ and $|1100\rangle$ are -1 , while the coefficient of $|0011\rangle$, $|0101\rangle$ and $|1001\rangle$ is 1. Then, we apply three CZ gates, and obtain

$$4U_{CZ}^{(13)}U_{CZ}^{(23)}U_{CZ}^{(12)}U_Z^{(1)}U_Z^{(2)}U_Z^{(3)}\psi_x = -(|0000\rangle + |0001\rangle + |0010\rangle + |0011\rangle + |0100\rangle + |0101\rangle + |0110\rangle + |0111\rangle + |1000\rangle + |1001\rangle + |1010\rangle + |1011\rangle + |1100\rangle + |1101\rangle - |1110\rangle - |1111\rangle) \quad (\text{A4})$$

(iii) We focus on the states $|n_1n_2n_3n_4\rangle$ such that $\sum_i n_i = 3$, among which the coefficients of $|1110\rangle$ is -1 , while the coefficient of $|0111\rangle$, $|1011\rangle$ and $|1101\rangle$ is 1. Then, we apply one CCZ gate, and obtain the equal-coefficient state,

$$4U_{CCZ}^{(123)}U_{CZ}^{(13)}U_{CZ}^{(23)}U_{CZ}^{(12)}U_Z^{(1)}U_Z^{(2)}U_Z^{(3)}\psi_x = -(|0000\rangle + |0001\rangle + |0010\rangle + |0011\rangle + |0100\rangle + |0101\rangle + |0110\rangle + |0111\rangle + |1000\rangle + |1001\rangle + |1010\rangle + |1011\rangle + |1100\rangle + |1101\rangle + |1110\rangle + |1111\rangle). \quad (\text{A5})$$

Hence, it follows from (60) that

$$V_x^{-1} = -U_{CCZ}^{(123)}U_{CZ}^{(13)}U_{CZ}^{(23)}U_{CZ}^{(12)}U_Z^{(1)}U_Z^{(2)}U_Z^{(3)}. \quad (\text{A6})$$

Consequently, $|\psi_x\rangle$ is obtained by the inverse process as

$$\psi_x = -U_{CCZ}^{(123)}U_{CZ}^{(13)}U_{CZ}^{(23)}U_{CZ}^{(12)}U_Z^{(1)}U_Z^{(2)}U_Z^{(3)} \bigotimes_{s=1}^4 U_H^{(s)} |0000\rangle, \quad (\text{A7})$$

because all $C^{p-1}Z$ gates are commutative and one $C^{p-1}Z$ gate U satisfies $U^2 = 1$.

In a similar way,

$$\psi_w = \frac{1}{4}(|0000\rangle + |0001\rangle - |0010\rangle - |0011\rangle - |0100\rangle + |0101\rangle + |0110\rangle + |0111\rangle + |1000\rangle + |1001\rangle + |1010\rangle + |1011\rangle + |1100\rangle + |1101\rangle + |1110\rangle + |1111\rangle) \quad (\text{A8})$$

is generated as

$$\psi_w = U_{CCCZ}^{(1234)}U_{CCZ}^{(124)}U_{CCZ}^{(234)}U_{CZ}^{(12)}U_{CZ}^{(13)}U_{CZ}^{(24)}U_Z^{(2)}U_Z^{(3)} \bigotimes_{s=1}^4 U_H^{(s)} |0000\rangle. \quad (\text{A9})$$

Thus, it is a nontrivial problem to construct hypergraph generation circuits in the standard quantum-circuit implementation.

Appendix B: Number recognition

We show binary representations of the pattern of each number for the reference and the input data in Fig.8, where the left hand side stands for the reference and the right one for the input data,

$$\begin{array}{ll} 0 : (11111001100110011111), & (01101001100110010110), \\ 1 : (01101010001000101111), & (01100010001000100010), \\ 2 : (11111001001001001111), & (01110001001001000111), \\ 3 : (01101001001010010110), & (11111001001010011111), \\ 4 : (10101010111100100010), & (00101010111000100010), \\ 5 : (11111000111100011111), & (01101000111000011110), \\ 6 : (11111000111110011111), & (01101000111010011110), \\ 7 : (11110001001000100100), & (01100001001000100010), \\ 8 : (11111001111100111111), & (01101001011010010110), \\ 9 : (11111001111100011111), & (01101001011100010110), \end{array} \quad (\text{B1})$$

where 0 indicates a white pixel and 1 indicates a black pixel.

- ¹ R. Feynman, *Int. J. Theor. Phys.* 21, 467 (1982).
- ² D. P. DiVincenzo, *Science* 270, 255 (1995).
- ³ M. Nielsen and I. Chuang, "Quantum Computation and Quantum Information", Cambridge University Press, (2016); ISBN 978-1-107-00217-3.
- ⁴ Y. Nakamura; Yu. A. Pashkin; J. S. Tsai, *Nature* 398, 786 (1999).
- ⁵ E. Knill, R. Laflamme and G. J. Milburn, *Nature*, 409, 46 (2001).
- ⁶ D. Loss and D. P. DiVincenzo, *Phys. Rev. A* 57, 120 (1998).
- ⁷ J. I. Cirac and P. Zoller, *Phys. Rev. Lett.* 74, 4091 (1995).
- ⁸ L. M.K. Vandersypen, M. Steffen, G. Breyta, C. S. Yannoni, M. H. Sherwood, I. L. Chuang, *Nature* 414, 883 (2001).
- ⁹ B. E. Kane, *Nature* 393, 133 (1998).
- ¹⁰ D. Deutsch, *Proceedings of the Royal Society A.* 400, 97 (1985).
- ¹¹ C. M. Dawson and M. A. Nielsen arXiv:quant-ph/0505030.
- ¹² M. Nielsen and I. Chuang, "Quantum Computation and Quantum Information", Cambridge University Press, Cambridge, UK (2010).
- ¹³ C. H. Lee, S. Imhof, C. Berger, F. Bayer, J. Brehm, L. W. Molenkamp, T. Kiessling and R. Thomale, *Communications Physics*, 1, 39 (2018).
- ¹⁴ S. Imhof, C. Berger, F. Bayer, J. Brehm, L. Molenkamp, T. Kiessling, F. Schindler, C. H. Lee, M. Greiter, T. Neupert, R. Thomale, *Nat. Phys.* 14, 925 (2018).
- ¹⁵ M. S.-Garcia, R. Susstrunk and S. D. Huber, *Phys. Rev. B* 99, 020304 (2019).
- ¹⁶ T. Helbig, T. Hofmann, C. H. Lee, R. Thomale, S. Imhof, L. W. Molenkamp and T. Kiessling, *Phys. Rev. B* 99, 161114 (2019).
- ¹⁷ E. I. Rosenthal, N. K. Ehrlich, M. S. Rudner, A. P. Higginbotham, and K. W. Lehnert, *Phys. Rev. B* 97, 220301(R) (2018).
- ¹⁸ Y. Lu, N. Jia, L. Su, C. Owens, G. Juzeliunas, D. I. Schuster and J. Simon, *Phys. Rev. B* 99, 020302 (2019).
- ¹⁹ M. Ezawa, *Phys. Rev. B* 98, 201402(R) (2018).
- ²⁰ Y. Li, Y. Sun, W. Zhu, Z. Guo, J. Jiang, T. Kariyado, H. Chen and X. Hu, *Nat. Com.* 9, 4598 (2018).
- ²¹ T. Hofmann, T. Helbig, C. H. Lee, M. Greiter, R. Thomale, *Phys. Rev. Lett.* 122, 247702 (2019).
- ²² K. Luo, R. Yu and H. Weng, *Research* (2018), ID 6793752.
- ²³ M. Ezawa, *Phys. Rev. B* 99, 201411(R) (2019).
- ²⁴ M. Ezawa, *Physical Review B* 99 (12), 121411 (2019).
- ²⁵ M. Ezawa, *Phys. Rev. B* 100, 045407 (2019).
- ²⁶ T. Helbig, T. Hofmann, S. Imhof, M. Abdelghany, T. Kiessling, L. W. Molenkamp, C. H. Lee, A. Szameit, M. Greiter, R. Thomale, *Nature Physics*, 16, 747 (2020).
- ²⁷ M. Ezawa, *Phys. Rev. Research* 2, 023278 (2020).
- ²⁸ M. Ezawa, *J. Phys. Soc. Jpn.* 89, 124712 (2020).
- ²⁹ M. Ezawa, *Phys. Rev. B* 102, 075424 (2020).
- ³⁰ M. Ezawa, *Phys. Rev. B* 100, 165419 (2019).
- ³¹ S. Lloyd, M. Mohseni and P. Rebentrost, arXiv:1307.0411.
- ³² M. Schuld, I. Sinayskiy, F. Petruccione, *Contemporary Physics* 56, 172 (2014).
- ³³ J. Biamonte, *Nature*. 549, 195 (2017).
- ³⁴ P. Wittek, "Quantum Machine Learning: What Quantum Computing Means to Data Mining", Academic Press (2014); ISBN 978-0128100400.
- ³⁵ A. W. Harrow, A. Hassidim and S. Lloyd, *Phys. Rev. Lett.* 103, 150502 (2009).
- ³⁶ N. Wiebe, D. Braun and S. Lloyd, *Phys. Rev. Lett.* 109, 050505 (2012).
- ³⁷ P. Rebentrost, M. Mohseni, S. Lloyd, *Phys. Rev. Lett.* 113, 130503 (2014).
- ³⁸ Z. Li, X. Liu, N. Xu and J. Du, *Phys. Rev. Lett.* 114, 140504 (2015).
- ³⁹ M. Schuld and N. Killoran, *Phys. Rev. Lett.* 122, 040504 (2019).
- ⁴⁰ V. Havlicek, A. D. Corcoles, K. Temme, A. W. Harrow, A. Kandala, J. M. Chow and J. M. Gambetta, *Nature* 567, 209 (2019).
- ⁴¹ *Mach. Learn.: Sci. Technol.* 1, 033002 (2020).
- ⁴² I. Cong, S. Choi and M. D. Lukin, *Nature Physics* 15, 1273 (2019).
- ⁴³ J. Schmidhuber, *Neural Netw.* 61, 85 (2015).
- ⁴⁴ J. M. Zurada, "Introduction to Artificial Neural Systems", West Group, St. Paul, MN, USA, (1992); ISBN 978-0314933911.
- ⁴⁵ M. Schuld, I. Sinayskiy and F. Petruccione, *Phys. Lett. A* 379, 660 (2015).
- ⁴⁶ N. Wiebe, A. Kapoor and K. N. Svore, arXiv:1602.04799.
- ⁴⁷ Y. Cao, G. G. Guerreschi and A. Aspuru-Guzik, arXiv:1711.11240.
- ⁴⁸ F. Tacchino, C. Macchiavello, D. Gerace and D. Bajoni, *npj quantum information* 5:26 (2019).
- ⁴⁹ E. Torrontegui and J. J. Garcia-Ripoll, *EPL* 125, 30004 (2019).
- ⁵⁰ L. B. Kristensen, M. Degroote, P. Wittek, A. Aspuru-Guzik and N. T. Zinner, arXiv:1907.06269.
- ⁵¹ N. Killoran, T. R. Bromley, J. M. Arrazola, M. Schuld, N. Quesada and S. Lloyd, *Phys. Rev. Res.* 1, 033063 (2019).
- ⁵² S. Mangini, F. Tacchino, D. Gerace, C. Macchiavello and D. Bajoni, *Mach. Learn.: Sci. Technol.* 1 045008 (2020).
- ⁵³ D. Deutsch and R. Jozsa, *Proc. R. Soc. Lond. A* 439, 553 (1992).
- ⁵⁴ L. Grover, *Proc. 28th Annual ACM Symposium on the Theory of Computing*, 212 (1996).
- ⁵⁵ M. Rossi, M. Huber, D. Bruss and C. Macchiavello, *New J. Phys.* 15 113022 (2013).
- ⁵⁶ F. Rosenblatt, *Tech. Rep. Inc. Report No. 85-460-1*, Cornell Aeronautical Laboratory (1957).
- ⁵⁷ W. S. McCulloch and W. Pitts, *Bull. Math. Biophys.* 5, 115 (1943).
- ⁵⁸ X. Glorot, A. Bordes and Y. Bengio, *Proceedings of the Fourteenth International Conference on Artificial Intelligence and Statistics (AISTATS-11)* 15: 315.
- ⁵⁹ M. Hein, J. Eisert, and H. J. Briegel, *Phys. Rev. A* 69, 062311 (2004).
- ⁶⁰ M. Hein, W. D. J. Eisert, R. Raussendorf, M. Van den Nest, H.-J. Briegel, "Entanglement in Graph States and its Applications", *Proceedings of the International School of Physics "Enrico Fermi" on "Quantum Computers, Algorithms and Chaos"*.
- ⁶¹ S. Anders and H. J. Briegel, *Phys. Rev. A* 73, 022334 (2006).
- ⁶² R. Qu, J. Wang, Z.-S. Li and Y.-R. Bao, *Phys. Rev. A* 87, 022311 (2013).